LETTER

doi:10.1038/nature10879

Phase transitions in the assembly of multivalent signalling proteins

Pilong Li[1]*, Sudeep Banjade[1]*, Hui-Chun Cheng[1]*, Soyeon Kim[1], Baoyu Chen[1], Liang Guo[2], Marc Llaguno[3], Javoris V. Hollingsworth[4], David S. King[5], Salman F. Banani[1], Paul S. Russo[4], Qiu-Xing Jiang[3], B. Tracy Nixon[6] & Michael K. Rosen[1]

Cells are organized on length scales ranging from ångström to micrometres. However, the mechanisms by which ångström-scale molecular properties are translated to micrometre-scale macroscopic properties are not well understood. Here we show that interactions between diverse synthetic, multivalent macromolecules (including multi-domain proteins and RNA) produce sharp liquid–liquid-demixing phase separations, generating micrometre-sized liquid droplets in aqueous solution. This macroscopic transition corresponds to a molecular transition between small complexes and large, dynamic supramolecular polymers. The concentrations needed for phase transition are directly related to the valency of the interacting species. In the case of the actin-regulatory protein called neural Wiskott–Aldrich syndrome protein (N-WASP) interacting with its established biological partners NCK and phosphorylated nephrin[1], the phase transition corresponds to a sharp increase in activity towards an actin nucleation factor, the Arp2/3 complex. The transition is governed by the degree of phosphorylation of nephrin, explaining how this property of the system can be controlled to regulatory effect by kinases. The widespread occurrence of multivalent systems suggests that phase transitions may be used to spatially organize and biochemically regulate information throughout biology.

Covalent and non-covalent interactions between multivalent small molecules are central elements of classical polymer chemistry and physics and of supramolecular chemistry[2–4]. These fields have produced theories and experimental demonstrations of sharp transitions between small assemblies and macroscopic polymer gels (known as sol–gel transitions) as the degree of bonding increases. The transition point (critical point) depends on the physical properties of the monomeric species, including valency and affinity. The polymer can have a variety of physical forms, ranging from phase-separated liquid to crystalline solid. For non-covalent systems, phase separation can strongly influence the sol–gel transition by altering the degree of bonding[5,6]. In biology, interactions between multivalent entities are found in diverse processes, including extracellular carbohydrate–lectin binding, intracellular signalling, RNA metabolism and chromatin organization in the nucleus[7–10]. Biological multivalency has been studied most extensively in the context of extracellular ligands binding to cell surface receptors, where antibody–receptor[11] and carbohydrate–lectin[7] systems can assemble into crosslinked networks. These networks are typically precipitates[11,12], but liquid-like gels have also been described[13]. Multivalency has been less studied in the context of intracellular molecules, which often share the characteristics of high valency, modest affinity, and long, flexible connections between binding elements[14]. Here we asked whether these systems also undergo sharp transitions to polymers, and if so, what the macroscopic properties of the polymers are and how such transitions could be regulated and affect function.

Initially, we examined interactions between the SRC homology 3 (SH3) domain and its proline-rich motif (PRM) ligand, two widely observed modules that often appear in tandem arrays in signalling proteins[8,14]. We generated two classes of engineered proteins: one composed of repeats of a single SH3 domain ($SH3_m$, where $m = 1–5$), and the other composed of repeats of a PRM ligand (PRM_n, where $n = 1–5$) (dissociation constant (K_d) = 350 μM for the $SH3_1$–PRM_1 interaction; Supplementary Fig. 1). Initially, we mixed $SH3_4$ with PRM_4. At low concentrations, the solutions were clear; by contrast, at high concentrations, they were opalescent. Examination of these opalescent solutions using light microscopy showed the presence of numerous spherical droplets of approximately 1 μm to >50 μm in diameter that had phase-separated from the bulk solution (Fig. 1a and Supplementary Fig. 2). Smaller droplets tended to coalesce into larger droplets over time, which is consistent with liquid-like properties (Fig. 1b). When the proteins were mixed in a 1:1 ratio, both the droplet and bulk phases contained equal amounts of each molecule, but the proteins were concentrated by about 100-fold in the droplets relative to

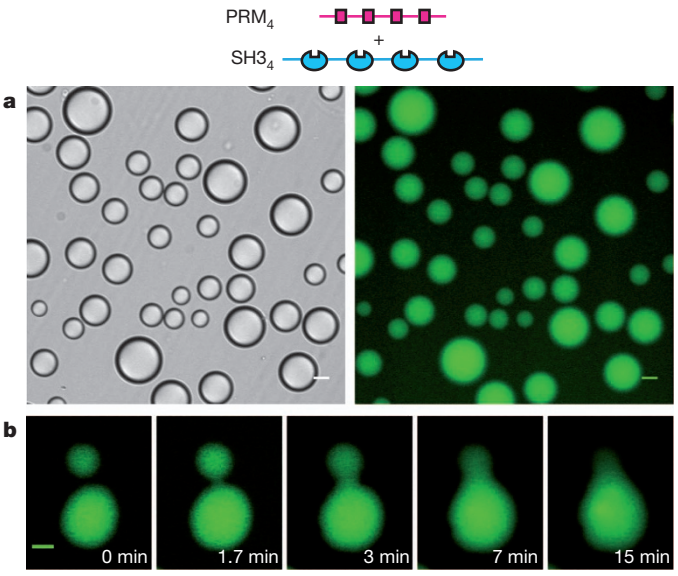

Figure 1 | Macroscopic and microscopic phase transitions in multivalent SH3–PRM systems. a, Liquid droplets observed by differential interference contrast microscopy (left) and wide-field fluorescence microscopy (right) when 300 μM $SH3_4$, 300 μM PRM_4 (both of which are module concentrations; molecule concentrations are 75 μM) and 0.5 μM OG–$SH3_4$ were mixed. Scale bars, 20 μm. **b**, Time-lapse imaging of merging droplets that were formed as in **a**. Scale bar, 10 μm.

[1]Department of Biochemistry and Howard Hughes Medical Institute, University of Texas Southwestern Medical Center, Dallas, Texas 75390-8812, USA. [2]BioCAT of IIT at the Advanced Photon Source, Argonne National Laboratory, 9700 South Cass Avenue, Argonne, Illinois 60439, USA. [3]Department of Cell Biology, University of Texas Southwestern Medical Center, Dallas, Texas 75390-9148, USA. [4]Department of Chemistry and Macromolecular Studies Group, Louisiana State University, Baton Rouge, Louisiana 70803, USA. [5]Howard Hughes Medical Institute Mass Spectrometry Laboratory and Department of Molecular & Cell Biology, University of California, Berkeley, California 94720, USA. [6]Department of Biochemistry and Molecular Biology, The Pennsylvania State University, University Park, Pennsylvania 16802, USA.

*These authors contributed equally to this work.

the bulk phase (Fig. 1a, right; 116-fold for $SH3_5$ plus PRM_5; and 82-fold for $SH3_5$ plus an octameric dendrimer, $PRM(N\text{-}WASP)_8$). Analogous droplets were also observed for an unrelated $SH3_5$–$ligand_5$ pair and for the tetravalent RNA binding protein PTB interacting with an RNA oligonucleotide (Supplementary Fig. 3). Thus, liquid–liquid-demixing phase transitions may occur in many multivalent intracellular systems.

A large body of data indicates that the phase separation observed here is driven by the assembly of the multivalent proteins into large species, analogous to the behaviour observed in many small-molecule polymer systems[2,5] as well as in covalent protein crosslinking[15]. First, the phase boundary is strongly dependent on the valency of the interacting species (Fig. 2a and Supplementary Fig. 4). This observation is consistent with theory and our simulations, which indicate that a higher valency allows the formation of larger species at a lower fractional saturation of the binding modules[2,3,5,16] (Supplementary Information and Supplementary Figs 5–7).

Second, the phase transition can be blocked by a high-affinity monovalent ligand, $PRM(H)_1$ ($K_d = 10\,\mu M$ for $SH3_1$ binding to $PRM(H)_1$; Supplementary Fig. 8). Third, we used dynamic light scattering (DLS) and small-angle X-ray scattering (SAXS) to characterize the species that formed during titrations of PRM proteins into $SH3_5$ (Fig. 2b and Supplementary Figs 10–12). At concentrations below those needed for droplet formation, the addition of either PRM_2 or PRM_4 substantially increased the apparent hydrodynamic radius (R_h, for DLS) and the apparent radius of gyration (R_g, for SAXS), suggesting that oligomeric species formed. For equal total module concentrations, PRM_4 caused larger increases in these values than did PRM_2, consistent with predictions from polymer theory[2,3,5,16]. For higher concentrations of PRM proteins, we removed the droplets by centrifugation and found that increasing the concentration of PRM_2 or PRM_4 caused R_h and R_g to decrease in the bulk phase, suggesting that larger species partitioned selectively into the droplet phase. This behaviour resembles that observed in the sol–gel transitions of covalent polymers, in which, above the critical extent of reaction, the average size of oligomers in the sol phase decreases because larger species preferentially join the gel[2]. Titrations of PRM_1 or $PRM(H)_1$, which unlike PRM_2 and PRM_4 cannot generate polymers and did not cause phase separation, produced only small, saturable increases in R_h and R_g. Taken together, these data indicate that phase separation is driven by the unique ability of multivalent $SH3_m$–PRM_n interactions to create large assemblies.

Additional lines of evidence suggest that the multivalent proteins formed large polymers within the droplets, such that the phase transition probably coincides with a sol–gel transition. First, at the extremely high concentrations in the droplet phase, the fractional saturation of SH3 and PRM binding sites is estimated to be threefold to fivefold higher than that needed to induce the sol–gel transition[16] (Supplementary Materials, Cyclization).

Second, DLS analyses of the droplet phases created by mixing $SH3_m$ and PRM_n showed multiphase intensity autocorrelation curves with a complex distribution of relaxation times spanning 0.2–20 ms (Supplementary Fig. 13) or longer (Fig. 2c). Some of these relaxation times nonlinearly scale with the square of the scattering angle (q^2) (Supplementary Fig. 13). The wide range of timescales, the presence of long-timescale processes and the q^2 independence of some of these processes are properties that are typical of polymer solutions in the semi-dilute range but are highly atypical of discrete molecular species[17].

Third, photobleaching experiments showed that the diffusion of the droplet constituents was slowed by about three orders of magnitude relative to free diffusion in water (data not shown). Furthermore, the photobleaching recovery rate correlated inversely with the monomer–monomer affinity and valency (Supplementary Fig. 14), suggesting that recovery represents reorganization of a polymer matrix. Small-molecule fluorophores and enhanced green fluorescent protein (eGFP) can enter, and move rapidly within, the droplets (Supplementary Fig. 15).

Last, cryo-electron microscopy images of $SH3_5$ plus PRM_5 solutions that were flash-frozen immediately after mixing showed numerous round, electron-dense objects with diameters of about 50–500 nm (Fig. 2d and Supplementary Fig. 16). These objects were not observed with high concentrations of either $SH3_5$ or PRM_5 alone or when the two components were mixed at concentrations below the droplet concentration. Although the objects were too dense for structures to be observed within them, their edges were highly irregular on the ~10-nm scale, suggesting that they contained large but disordered molecular species, consistent with a crosslinked gel. These characterizations of the droplet phase suggest that this phase contains large polymeric species and has undergone a sol–gel transition.

Taken together, our data suggest a model in which the association of multivalent proteins produces a macroscopic liquid–liquid phase separation, which is thermodynamically coupled to a molecular sol–gel transition within the droplet phase. The sharp transition between small complexes and polymers is consistent with condensation polymerization theory[2,3,6] and our own particle-based simulations (Supplementary Fig. 5). A theoretical analysis of these systems (Supplementary Information) indicates that the polymerization process is driven appreciably by the extremely high configurational entropy of the polymer[6,18].

The behaviour that we observed for these multivalent systems *in vitro* was mirrored in cells. The coexpression of mCherry–$SH3_5$ and eGFP–PRM_5 fusion proteins in HeLa cells resulted in the formation of approximately 0.5–2-μm diameter cytoplasmic puncta containing both fluorophores (Fig. 3a). Puncta were not observed in cells expressing either protein alone or in cells coexpressing mCherry–$SH3_5$ and eGFP–PRM_3, indicating that their formation depends on the interaction between the two high-valency molecules. The puncta did not stain with a large range of vesicle markers or a lipid dye, suggesting that they are phase-separated bodies rather than vesicular structures (Supplementary Fig. 18). Both mCherry and eGFP fluorescence of the bodies recovered within about 10 s of photobleaching (Fig. 3b), indicating that there was rapid exchange of both components with the

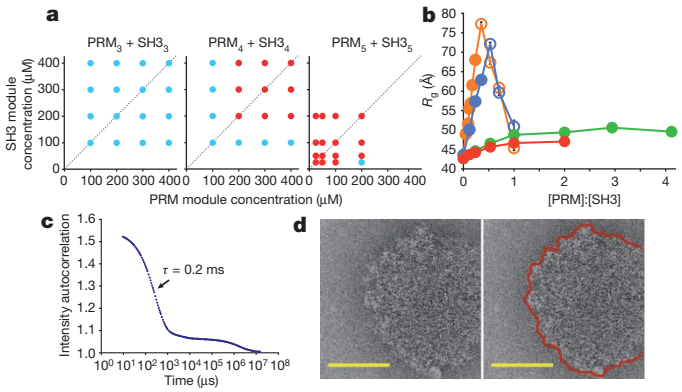

Figure 2 | Multivalency drives phase separation and probably drives a sol–gel transition in the droplet phase. **a**, Phase diagrams of multivalent SH3 and PRM proteins. The concentrations are in terms of the modules. The red circles indicate phase separation, and the blue circles indicate no phase separation. **b**, The R_g values determined from SAXS data that were collected during titrations of PRM proteins into $SH3_5$. Closed circles indicate the absence of phase separation; open circles indicate data collected on the supernatant phase, which was separated from the droplets by centrifugation. The titrations used PRM_4 (orange), PRM_2 (blue), PRM_1 (green) and $PRM(H)_1$ (red). The error bars represent the s.d. calculated from five to ten independent measurements of intensity versus scattering angle (q). **c**, The intensity autocorrelation curve of light scattered at 90° from the pooled droplet phase of $SH3_5$ plus $PRM(N\text{-}WASP)_8$. τ, the relaxation time constant of the most rapidly decaying phase. **d**, Cryo-electron microscopy image of a droplet formed by $SH3_5$ plus PRM_5 (identical image, left and right). The edge of the structure is outlined in red (right). Scale bars, 100 nm.

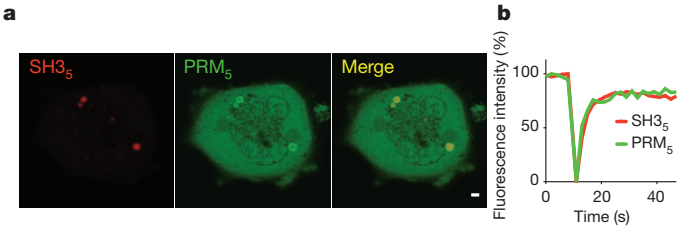

Figure 3 | Coexpression of $SH3_5$ and PRM_5 in cells produces dynamic puncta. **a**, mCherry–$SH3_5$ (left), eGFP–PRM_5 (centre) and an image overlay in a cell expressing both proteins (right). It should be noted that the non-uniform eGFP fluorescence in the puncta results from mCherry–eGFP fluorescence resonance energy transfer (FRET) rather than from differential localization of the proteins (Supplementary Fig. 17). Scale bar, 2 μm. **b**, Both mCherry and eGFP fluorescence recover rapidly after photobleaching.

surrounding cytoplasm and suggesting that the bodies had a dynamic liquid-like nature. Thus, interactions between multivalent proteins can produce phase-separated liquid droplets both *in vitro* and in cells.

The nephrin–NCK–N-WASP system is a natural, three-component interaction that can be used to investigate phase transitions that result from multivalent interactions, as well as the functional consequences of these transitions (Fig. 4a). In kidney podocytes, the transmembrane protein nephrin plays a central role in forming the glomerular filtration barrier, functioning partly through assembling cortical actin[1]. The cytoplasmic tail of nephrin contains three tyrosine phosphorylation (pTyr) sites, which can each bind the SH2 domain of NCK[1,19]. NCK contains three SH3 domains, which can bind the six PRMs in the proline-rich region of N-WASP[20]. N-WASP, in turn, stimulates the nucleation of actin filaments by the Arp2/3 complex. The multivalency of nephrin or NCK is necessary for proper actin assembly[19] and, together with the multivalency of N-WASP, has the potential to cause phase transitions.

The addition of NCK to an N-WASP construct (GBD-P-VCA, Supplementary Table 1; called N-WASP hereafter) caused droplet formation, as occurred in the model systems described above (Fig. 4b). The addition of a diphosphorylated (2pTyr) nephrin tail peptide dropped the phase boundary for both proteins by more than or equal to twofold (Fig. 4c), presumably because the effective valency of NCK increases when it is arrayed on nephrin. This effect was even more pronounced when nephrin–3pTyr peptide was added (to the same total pTyr concentration) (Fig. 4d). Thus, in cells, protein kinases could regulate phase transitions in this system (and the cooperative assembly of all three proteins) by controlling the degree of phosphorylation of nephrin and, consequently, by shifting the phase boundary from the micromolar (Fig. 4b) to the nanomolar (Fig. 4d) regime. It should be noted that, where measured, the cytoplasmic concentrations of WASP proteins and other actin-regulatory molecules were typically 1–10 μM, indicating that shifts in this range could be functionally important (Supplementary Fig. 19).

We next asked how droplet formation affects the ability of the nephrin–NCK–N-WASP system to stimulate Arp2/3-mediated actin assembly. We measured the half-time to completion ($t_{1/2}$) of pyrene–actin assembly reactions containing fixed concentrations of the Arp2/3 complex, NCK, nephrin–3pTyr peptide and N-WASP plus variable amounts of an N-WASP truncation mutant (N-WASPΔ) that contains the full proline-rich region and can assemble into polymers but cannot bind the Arp2/3 complex. In the absence of N-WASPΔ, 50 nM N-WASP produced only weak stimulation of the Arp2/3 complex (long $t_{1/2}$) (Fig. 4e). The addition of N-WASPΔ to concentrations between 0 and 750 nM had no effect on actin assembly. However, 1,000 nM N-WASPΔ sharply increased the activation of the Arp2/3 complex. The activity increased asymptotically as the concentration of N-WASPΔ was raised further. N-WASPΔ had no effect on an N-WASP protein that lacks the proline-rich region, suggesting that

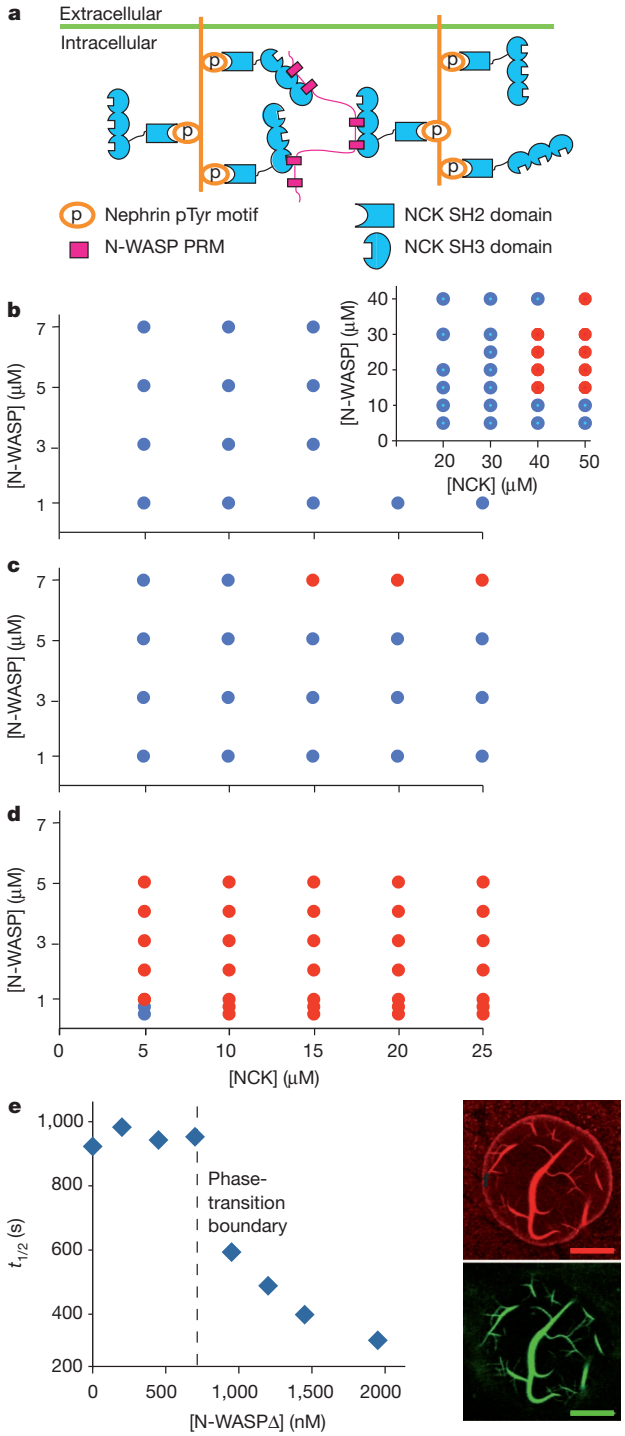

Figure 4 | Phase transition correlates with biochemical activity transition in the nephrin–NCK–N-WASP system. **a**, The interactions of nephrin, NCK and N-WASP. **b**–**d**, Phase diagrams of N-WASP and NCK alone (**b**, inset shows higher concentrations) or in the presence of 4.5 μM diphosphorylated nephrin tail peptides (**c**) or 3 μM triphosphorylated nephrin tail peptides (**d**). The red circles indicate phase separation, and the blue circles indicate no phase separation. **e**, The half-time to completion ($t_{1/2}$) of N-WASP-stimulated actin assembly by the Arp2/3 complex as a function of N-WASPΔ concentration. The vertical dashed line indicates the phase-separation boundary determined in separate assays without actin and the Arp2/3 complex. **f**, Rhodamine–actin (4 μM, 10% rhodamine-labelled), 300 nM Alexa-488–phalloidin and 10 nM Arp2/3 complex were added to droplets containing triphosphorylated nephrin, NCK and N-WASP, and the droplets were imaged by confocal microscopy; rhodamine (top) and Alexa 488 (bottom) are shown separately. Scale bars, 10 μm.

engagement by NCK is needed for the increase in activity (Supplementary Fig. 20).

These data are consistent with the switch-like formation of a higher activity[21,22] (probably polymeric) form of nephrin–NCK–N-WASP when the total concentration of wild-type (active) plus truncated (inactive) N-WASP surpasses that needed for droplet formation. The sharp transition was followed by slower increases in activity as additional N-WASPΔ drew a greater percentage of the wild-type protein into the droplets/polymer. Consistent with these ideas, when mixtures containing N-WASP above its phase-separation concentration were stained with phalloidin, numerous bundles of actin filaments were observed within the droplets (Fig. 4f). In cells, nephrin is a transmembrane protein, and the system would not produce a three-dimensional polymer phase as observed here but rather its two-dimensional equivalent at the plasma membrane. Such interactions might contribute to the formation and/or the stability of the micrometre-scale clusters of nephrin and NCK with the associated actin tails, which are observed in cells when nephrin is crosslinked (and subsequently phosphorylated)[1]. Of the 28 known binding partners of the NCK SH2 domain, 14 are predicted or have been demonstrated to contain three or more pTyr sites[23,24], suggesting that analogous pTyr–NCK–N-WASP assembly may occur in many systems.

Sharp phase transitions occurring concomitantly with sol–gel transitions may be a general feature of multivalent systems in biology. Many 'cellular bodies'—that is, subcellular compartments that are compositionally distinct from the surrounding cytoplasm or nucleoplasm but that are not membrane bounded[25,26]—are enriched in multivalent proteins and nucleic acids[9,27]. These include promyelocytic leukaemia nuclear bodies, Cajal bodies, P bodies and P granules[27–29]. Moreover, P granules in the *Caenorhabditis elegans* embryo were recently shown to have liquid-like properties with many of the features that we observed here, including switch-like formation and greatly slowed diffusion of constituent molecules[30]. Many multivalent proteins, in general, can organize into puncta in the cytosol or at membranes (Supplementary Fig. 21). Within puncta, the physical properties of a polymer could impart micrometre-scale structural and dynamic organization and control the chemistry (for example, of catalysis, molecular interactions or structural rearrangements). Our findings provide a mechanism by which multivalent interactions could yield sharp transitions between physically and functionally distinct states, generating nonlinearity in signalling pathways, connecting disparate length scales in the cell, and perhaps contributing to the structure and function of cellular bodies and other two- and three-dimensional compartments.

METHODS SUMMARY

Material generation. Details are provided in the Supplementary Information.

***In vitro* phase separation.** Samples were incubated for >12 h before scoring them for droplets using bright-field microscopy; when observed, the droplets formed immediately after mixing. For *in vitro* fluorescence recovery after photobleaching (FRAP) experiments, a 5-μm diameter spot was bleached in droplets of >20-μm diameter containing Oregon Green (OG)-labelled $SH3_4$ (OG–$SH3_4$) by using a 488-nm laser line. The mean intensity of the bleached spot was fit to a single exponential.

DLS and SAXS. For titrations monitored by DLS (DynaPro, Wyatt) and SAXS (Advanced Photon Source, Biophysics Collaborative Access Team (BioCAT) beamline), the samples contained 170 μM $SH3_5$ plus PRM proteins at PRM:SH3 module ratios of 0–5. Droplets were removed from all of the relevant samples by centrifugation (at 16,000*g* for 10 min) before analysis. For $SH3_5$ plus PRM(N-WASP)$_8$ and $SH3_5$ plus PRM_5 droplets, single-angle DLS data were collected on a DynaPro instrument, and multi-angle DLS data were collected on a custom-built apparatus.

Cryo-electron microscopy. The samples were blotted, frozen immediately after mixing and imaged under low-dose cryo conditions in a 2200FS FEG transmission electron microscope (JEOL), using a 2k × 2k slow-scan charge-coupled display (CCD) camera (Tietz).

Cellular assays. HeLa cells were imaged at 32 °C 24 h after transfection with vectors expressing mCherry–$SH3_5$ and/or eGFP–PRM_5 (or eGFP–PRM_3). Images were acquired on an LSM 510 confocal microscope (Zeiss). For FRAP experiments, individual puncta containing both mCherry–$SH3_5$ and eGFP–PRM_5 were bleached with a 488-nm laser line.

Actin polymerization. Actin (4 μM, 5% pyrene-labelled actin) was polymerized in the presence of 3 μM nephrin–3pTyr, 10 μM NCK, 50 nM N-WASP and 10 nM Arp2/3 complex plus increasing concentrations of N-WASPΔ in 150KMEI buffer (150 mM KCl, 1 mM $MgCl_2$, 1 mM EGTA and 10 mM imidazole, pH 7) as described previously[21]. Imaging was performed on an LSM 510 confocal microscope after adding rhodamine–actin (4 μM, 10% rhodamine-labelled actin), 300 nM Alexa 488–phalloidin and 10 nM Arp2/3 complex to droplets containing 3 μM nephrin–3pTyr, 10 μM NCK and 2 μM N-WASP.

Full Methods and any associated references are available in the online version of the paper at www.nature.com/nature.

Received 4 May 2010; accepted 20 January 2012.
Published online 7 March 2012.

1. Jones, N. *et al.* Nck adaptor proteins link nephrin to the actin cytoskeleton of kidney podocytes. *Nature* **440,** 818–823 (2006).
2. Flory, P. J. *Principles of Polymer Chemistry* (Cornell Univ. Press, 1953).
3. Cohen, R. J. & Benedek, G. B. Equilibrium and kinetic theory of polymerization and the sol-gel transition. *J. Phys. Chem.* **86,** 3696–3714 (1982).
4. Lehn, J.-M. Supramolecular polymer chemistry—scope and perspectives. *Polym. Int.* **51,** 825–839 (2002).
5. Tanaka, F. *Polymer Physics: Applications to Molecular Association and Thermoreversible Gelation* (Cambridge Univ. Press, 2011).
6. Semenov, A. N. & Rubinstein, M. Thermoreversible gelation in solutions of associative polymers. 1. Statics. *Macromolecules* **31,** 1373–1385 (1998).
7. Brewer, C. F., Miceli, M. C. & Baum, L. G. Clusters, bundles, arrays and lattices: novel mechanisms for lectin–saccharide-mediated cellular interactions. *Curr. Opin. Struct. Biol.* **12,** 616–623 (2002).
8. Pawson, T. & Nash, P. Assembly of cell regulatory systems through protein interaction domains. *Science* **300,** 445–452 (2003).
9. Lunde, B. M., Moore, C. & Varani, G. RNA-binding proteins: modular design for efficient function. *Nature Rev. Mol. Cell Biol.* **8,** 479–490 (2007).
10. Ruthenburg, A. J., Li, H., Patel, D. J. & Allis, C. D. Multivalent engagement of chromatin modifications by linked binding modules. *Nature Rev. Mol. Cell Biol.* **8,** 983–994 (2007).
11. Goldberg, R. A theory of antibody–antigen reactions. I. Theory for reactions of multivalent antigen with bivalent and univalent antibody. *J. Am. Chem. Soc.* **74,** 5715–5725 (1952).
12. Dam, T. K. *et al.* Thermodynamic, kinetic, and electron microscopy studies of concanavalin A and *Dioclea grandiflora* lectin cross-linked with synthetic divalent carbohydrates. *J. Biol. Chem.* **280,** 8640–8646 (2005).
13. Sisu, C. *et al.* The influence of ligand valency on aggregation mechanisms for inhibiting bacterial toxins. *Chembiochem* **10,** 329–337 (2009).
14. Jin, J. *et al.* Eukaryotic protein domains as functional units of cellular evolution. *Sci. Signal.* **2,** ra76 (2009).
15. Asherie, N. *et al.* Oligomerization and phase separation in globular protein solutions. *Biophys. Chem.* **75,** 213–227 (1998).
16. Stockmayer, W. H. Molecular distribution in condensation polymers. *J. Polym. Sci.* **9,** 69–71 (1952).
17. Li, J., Ngai, T. & Wu, C. The slow relaxation mode: from solutions to gel networks. *Polym. J.* **42,** 609–625 (2010).
18. Semenov, A., Charlot, A., Auzely-Velty, R. & Rinaudo, M. Rheological properties of binary associating polymers. *Rheol. Acta* **46,** 541–568 (2007).
19. Blasutig, I. M. *et al.* Phosphorylated YDXV motifs and Nck SH2/SH3 adaptors act cooperatively to induce actin reorganization. *Mol. Cell. Biol.* **28,** 2035–2046 (2008).
20. Rohatgi, R., Nollau, P., Ho, H. Y., Kirschner, M. W. & Mayer, B. J. Nck and phosphatidylinositol 4,5-bisphosphate synergistically activate actin polymerization through the N-WASP–Arp2/3 pathway. *J. Biol. Chem.* **276,** 26448–26452 (2001).
21. Padrick, S. B. *et al.* Hierarchical regulation of WASP/WAVE proteins. *Mol. Cell* **32,** 426–438 (2008).
22. Padrick, S. B. & Rosen, M. K. Physical mechanisms of signal integration by WASP family proteins. *Annu. Rev. Biochem.* **79,** 707–735 (2010).
23. Lettau, M., Pieper, J. & Janssen, O. Nck adaptor proteins: functional versatility in T cells. *Cell Commun. Signal.* **7,** 1 (2009).
24. Obenauer, J. C., Cantley, L. C. & Yaffe, M. B. Scansite 2.0: proteome-wide prediction of cell signaling interactions using short sequence motifs. *Nucleic Acids Res.* **31,** 3635–3641 (2003).
25. Matera, A. G., Izaguire-Sierra, M., Praveen, K. & Rajendra, T. K. Nuclear bodies: random aggregates of sticky proteins or crucibles of macromolecular assembly? *Dev. Cell* **17,** 639–647 (2009).
26. Buchan, J. R. & Parker, R. Eukaryotic stress granules: the ins and outs of translation. *Mol. Cell* **36,** 932–941 (2009).
27. Parker, R. & Sheth, U. P bodies and the control of mRNA translation and degradation. *Mol. Cell* **25,** 635–646 (2007).
28. Matera, A. G. & Shpargel, K. B. Pumping RNA: nuclear bodybuilding along the RNP pipeline. *Curr. Opin. Cell Biol.* **18,** 317–324 (2006).
29. Bernardi, R. & Pandolfi, P. P. Structure, dynamics and functions of promyelocytic leukaemia nuclear bodies. *Nature Rev. Mol. Cell Biol.* **8,** 1006–1016 (2007).

30. Brangwynne, C. P. *et al.* Germline P granules are liquid droplets that localize by controlled dissolution/condensation. *Science* **324,** 1729–1732 (2009).

Supplementary Information is linked to the online version of the paper at www.nature.com/nature.

Acknowledgements We thank J. Onuchic and S. Padrick for discussion of the theoretical aspects of this study, L. Rice for sharing his fluorescence microscope, M. Socolich for a gift of purified eGFP, K. Luby-Phelps and A. Bugde for advice on FRAP experiments, S. Padrick and L. Doolittle for help in purifying actin and the Arp2/3 complex and for sharing reagents, N. Grishin and S. Shi for help with database searches, K. Lynch for providing the PTB expression construct, D. Billadeau and T. Gomez for providing antibodies, A. Ramesh, W. Winkler and P.-L. Tsai for advice on RNA experiments, K. Roybal and C. Wülfing for sharing unpublished data, and J. Liu for help with cryo-electron tomography. This work was supported by the following: the Howard Hughes Medical Institute and grants from the National Institutes of Health (NIH) (R01-GM56322) and Welch Foundation (I–1544) to M.K.R., a Chilton Foundation Fellowship to H.-C.C., an NIH EUREKA award (R01-GM088745) to Q.-X.J., an NIH Cancer Biology T32 Training Grant to M.L., a National Science Foundation award (DMR-1005707) to P.S.R. and a Gates Millennium Fund award to J.V.H. Use of the Advanced Photon Source was supported by the US Department of Energy, Basic Energy Sciences, Office of Science, under contract number W-31-109-ENG-38. BioCAT is NIH-supported Research Center RR-08630.

Author Contributions M.K.R. oversaw the project, helped analyse all of the data and wrote the paper with assistance from all of the authors. P.L., H.-C.C. and M.K.R. conceived of the project. P.L. developed and interpreted the theoretical and computational models, which promoted much of the experimentation. S.B. performed and analysed experiments on the nephrin–NCK–N-WASP system and performed monovalent competition studies. H.-C.C. mapped and analysed the phase diagrams, and collected FRAP data, on the engineered model systems. S.K. performed and analysed the cellular experiments. S.B., B.C., L.G. and B.T.N. collected and/or analysed the SAXS data. S.B., M.L. and Q.-X. J. collected and/or analysed the electron microscopy data. S.B., J.V.H. and P.S.R. collected and/or analysed the multi-angle DLS data. H.-C.C. and S.B. collected and analysed the single-angle DLS data. D.S.K. synthesized the octameric PRM dendrimer. S.F.B. analysed the cyclization in the sol–gel transition.

Author Information Reprints and permissions information is available at www.nature.com/reprints. The authors declare no competing financial interests. Readers are welcome to comment on the online version of this article at www.nature.com/nature. Correspondence and requests for materials should be addressed to M.K.R. (Michael.Rosen@utsouthwestern.edu).

METHODS

Measurements of protein stoichiometry and concentration in droplets. All phase-separation assays were performed in 150KMEI buffer (150 mM KCl, 1 mM $MgCl_2$, 1 mM EGTA and 10 mM imidazole, pH 7), except where indicated. $SH3_4$ and PRM_4 (doped with 0.5% of either protein labelled with Oregon Green) were incubated at a 1:1 stoichiometry at various concentrations at room temperature overnight. The droplet phase (where formed) was collected by centrifugation, and the supernatant was removed and digested with proteinase K (Promega) overnight. The fluorescence intensity (excitation wavelength (λ_{ex}) = 488 nm, and emission wavelength (λ_{em}) = 512–521 nm) of the samples was converted to concentration using a standard curve of Oregon Green alone. The data revealed a 1:1 stoichiometry in all cases in both the droplet and the supernatant phases. In other systems that were mixed at a 1:1 module ratio, we calculated the concentrations from the absorbance at 280 nm using module-weighted extinction coefficients, assuming a 1:1 module stoichiometry in all phases.

SAXS. SAXS experiments were performed at the Biophysics Collaborative Access Team (BioCAT) undulator beamline 18-ID at the Advanced Photon Source, Argonne National Laboratory as described previously[31]. All samples were centrifuged for 10 min at 16,000*g* at 4 °C before mixing. In mixtures above the phase-transition concentration, solutions were centrifuged for an additional 10 min to remove the droplet phase before SAXS analysis. To minimize radiation damage, all samples were in 150KMEI buffer containing 5 mM TCEP and were flowed at 5 μl s^{-1} during data collection[31]. Scattering intensity profiles over the q range from 0.006 to 0.36 $Å^{-1}$ were calculated from radial averaging of the two-dimensional scattering patterns using macros written by the BioCAT staff for the software IGOR Pro (WaveMetrics). The scattering for each sample and the accompanying buffer were averaged from five to ten repeats, and the protein scattering was obtained by subtracting the buffer scattering. Guinier plots were used to calculate R_g and to ascertain the absence of aggregates. Alternatively, R_g and the distance distribution function, $P(r)$, were calculated using the program GNOM[32]. The apparent molecular weight was estimated[33] by integrating the Kratky plot to a maximum q at 0.2 $Å^{-1}$.

DLS titration. In the titration experiments, scattering measurements were performed on a DynaPro instrument (Wyatt) at 30% laser power and 22 °C. Twenty repetitive data sets, each of 100 s duration, were averaged for each titration point. Autocorrelation data were analysed using the regularization method in Dynamics version 6.4.3 software (Proterion Corporation). All samples were centrifuged before and after mixing, as for the SAXS titration.

DLS of $SH3_5$ plus $PRM(N\text{-}WASP)_8$ droplets. To collect enough volume of the droplet phase (~25 μl), 850 μM $SH3_5$ was mixed with 850 μM $PRM(N\text{-}WASP)_8$ (module concentrations) to a final volume of 900 μl in 150KMEI buffer. The denser, droplet, phase was collected by centrifugation (16,000*g* for 10 min) and analysed using a DynaPro instrument at 22 °C and 20% laser power. Twenty repetitive data sets, each of 1,000 s duration, were averaged.

Multi-angle DLS of $SH3_5$ plus PRM_5 droplet and supernatant phases. $SH3_5$ (850 μM) was mixed with PRM_5 (850 μM) (module concentrations) to a final volume of 900 μl to collect enough volume of the droplet phase (~20 μl). The denser, droplet, phase was collected by centrifugation. Measurements were made using a custom-built apparatus equipped with an Innova 90 argon laser (Coherent) set to 514.5 nm. A wide-range photometer–preamplifier–discriminator (Pacific Precision Instruments) drove a pulse shaper (ALV), which fed an ALV-5000 digital autocorrelator (ALV). The temperature was maintained at 25 °C by a circulating water bath. For the supernatant phase, three 10-min runs were collected and averaged at each scattering angle between 30° and 110°. For the droplet phase, a single 30-min run was collected at each angle. The distributions of the decay rate and the average decay rate were determined by analysing the correlation functions using an inverse Laplace transformation in the program CONTIN[34].

Cryo-electron microscopy. Carbon-coated copper grids were glow-discharged in an EMS-100 unit with a 40 mA current for 90 s. $SH3_5$ (100 μM) was loaded onto the grid, followed by PRM_5 (100 μM) (module concentrations), giving a 4 μl final volume. The mixture was immediately blotted for 6.5 s in a Vitrobot Mark III (Gatan) before being plunged into liquid ethane. Mixtures of $SH3_5$ and PRM_5 below the critical concentrations (2.5 μM module concentration each), or $SH3_5$ or PRM_5 alone (250 μM module concentration) were prepared identically. Samples contained 150KMEI buffer. Frozen grids were stored in liquid nitrogen until electron microscopy analysis. Imaging was performed under low-dose cryo conditions in a 2200FS FEG transmission electron microscope (JEOL), using a 2k × 2k slow-scan charge-coupled display (CCD) camera (Tietz). The dose rate was adjusted to ~20 electrons $Å^{-2}$ s^{-1}; the defocus level varied from −1.0 to −3.0 μm.

Cell culture and fluorescence microscopy. HeLa cells were cultured in Dulbecco's modified Eagle's medium (DMEM) containing 10% FBS. Cells were transfected using Effectene (QIAGEN) and incubated for 24 h at 37 °C. For Nile-Red staining, cells were incubated with Nile Red (at a final concentration of 0.5 μg ml^{-1}) for 15, 30 or 60 min before imaging. For immunofluorescence analysis, transfected cells were fixed with 4% paraformaldehyde in PBS and permeabilized with 0.1% Triton X-100 in PBS for 5 min. The antibodies used for staining were anti-EEA1, anti-GM130, anti-golgin-97, anti-VPS35, anti-CIMPR, anti-clathrin heavy chain, anti-LAMP1, anti-SNX1, anti-SNX2, anti-TGN46 (provided by D. Billadeau and T. Gomez) and anti-caveolin-1 antibodies. Secondary antibodies conjugated to Alexa Fluor 647 were obtained from Invitrogen. Images were collected on a DeltaVision system (Applied Precision). The mCherry–$SH3_5$ and eGFP–PRM_5 constructs were generated by cloning $SH3_5$ and PRM_5 into the vectors pmCherry-N1 and peGFP-N1, respectively. Images were processed using the program ImageJ (http://rsb.info.nih.gov/ij).

***In vitro* FRAP assays.** Fluorescence recovery after photobleaching (FRAP) experiments were performed on an LSM 510 confocal microscope (Zeiss) using a 488-nm laser line. The OG–$SH3_4$ or eGFP was bleached using ten iterative pulses (total time ~0.55 s) with full laser power. The droplets were >20 μm in diameter, and the bleached spots were 5 μm in diameter. The imaging power was 0.5% for OG–$SH3_4$ and 2% for eGFP. Images were processed using ImageJ. Background-corrected data were fit to a single exponential decay to yield the recovery time constant using GraphPad Prism 5 (GraphPad Software).

31. Chen, B. *et al.* ATP ground- and transition states of bacterial enhancer binding AAA+ ATPases support complex formation with their target protein, σ54. *Structure* **15,** 429–440 (2007).
32. Svergun, D. I. Determination of the regularization parameter in indirect-transform methods using perceptual criteria. *J. Appl. Crystallogr.* **25,** 495–503 (1992).
33. Fischer, H., Neto, M. O., Napolitano, H. B., Polikarpov, I. & Craievich, A. F. Determination of the molecular weight of proteins in solution from a single small-angle X-ray scattering measurement on a relative scale. *J. Appl. Crystallogr.* **43,** 101–109 (2010).
34. Provencher, S. W. CONTIN: a general purpose constrained regularization program for inverting noisy linear algebraic and integral equations. *Comput. Phys. Commun.* **27,** 229–242 (1982).